Article

CO$_2$ and CH$_4$ Adsorption Behavior of Biomass Based Activated Carbons

Deneb Peredo-Mancilla [1],* 0000-0001-5182-3523, **Imen Ghouma, Cecile Hort** [2], [3], **Camelia Matei Ghimbeu** [3], **Mejdi Jeguirim** [3] **and David Bessieres** [1],

[1]   CNRS/Total/Univ Pau & Pays Adour/ E2S UPPA, Laboratoire des Fluides Complexes et Leurs Reservoirs-IPRA, UMRS5150, 64000, Pau, France.
[2]   CNRS/Total/Univ Pau & Pays Adour/ E2S UPPA, Laboratoire de Thermique, Energetique et Procedes-IPRA, EA1932, 64000, Pau, France.
[3]   Institut de Sciences des Matériaux de Mulhouse, UMR 7661 CNRS, 15 rue Jean Starcky, 68057 Mulhouse, France.
*   Correspondence: peredo-mancilla.jd@univ-pau.fr

Abstract: The aim of the present study is to provide new insights into the CO$_2$ and CH$_4$ adsorption using a set of biomass-based activated carbons obtained by physical and chemical activation of olive-stones. The adsorption behavior is analyzed by means of pure gas adsorption isotherms up to 3.2 MPa at two temperatures (303.15 and 323.15 K).The influence of the activation method on the adsorption uptake is studied in terms of both textural properties and surface chemistry. For three activated carbons the CO$_2$ adsorption was more important than that of CH$_4$. The chemically activation resulted in higher BET surface area and micropore volume that lead to higher adsorption for both CO$_2$ and CH$_4$. For methane the presence of mesopores seems to facilitate the access of the gas molecules into the micropores while for carbon dioxide, the presence of oxygen groups enhanced the adsorption capacity.

Keywords: CO$_2$ adsorption, CH$_4$ adsorption, biomass, activated carbon.

1. Introduction

As part of the efforts being made to fight climate change, governments of 195 countries signed the Paris agreement in which they agreed to keep the increase in global average temperature well bellow 2°C from the preindustrial temperatures [1]. In order to meet with this target, the EU set a 20-20-20 goal: 20% increase in energy efficiency, 20% cut in greenhouse gas (GHG) emissions and 20% of EU energy from renewables by 2020. Furthermore, 10% of transportation fuels have to come from renewable sources such as biofuels [2].

Biogas is a gaseous mixture produced when organic matter is degadated by micro-organisms under anaerobic condition in a process known as anaerobic digestion (AD); its main components are methane (CH$_4$) in a concentration of 50 to 70%vol. and carbon dioxide (CO$_2$) ranging from 30 to 45% vol. Collected biogas can be directly burned to produce electricity with an efficiency of roughly 38% [3]. Alternatively, the energy density of biogas can be increased by an upgrading process in which the non-combustible gas (CO$_2$) and some present impurities are separated to produce a highly purified methane stream (around 98% purity) known as *biomethane* which can function as a vehicle fuel or be injected into the natural gas grid.

The use of biogas and biomethane as alternative energy source has gained attention, its implementation results in the reduction of greenhouse gases from both the burning of fossil fuels and from the landfill of organic wastes accounting for 3.2% of the total GHG emissions of the EU. In Europe more than 90% of the produced biogas is already being use for electricity generation and the upgrading of biogas is being more and more promoted [4]. EU energy production from biomethane rose from 752 GWh in 2011 to 17,264 GWh in 2016 (+16,512 GWh). Moreover, in 2016 biomethane production in Europe increased by 4,971 GWh (+40%) proving an accelerated development in the sector [5].

Adsorption based processes have been widely explored for the upgrading of biogas due to their relatively low energy requirements and capital investment cost, flexibility of design, safety and simplicity of operation, as well as a high efficiency [6]. On this type of separation technology, the components of a gas mixture are separated based on their molecular characteristics and affinity to an adsorbent material. For this purpose, a variety of materials have been studied including zeolites [7–9], carbon molecular sieves (CMS)[10–12], metal organic frameworks (MOFs) [13–15] and activated carbons (AC)[16–18].Among this materials, activated carbons present advantages in terms of (i) hydrophobicity, no need of water removal step before upgrading, (ii) low heat of adsorption, low energy of regeneration, (iii) possibility of heteroatoms functionalization to modify their adsorption behavior and (iv) high CO_2 adsorption capacity at ambient pressure [19]. Furthermore, activated carbons can be produced with a lower cost than other adsorbents, with a wide range of available precursor material.

The use of agro-industrial wastes as an alternative precursor material to coal and wood for activated carbon production has been widely studied [20–23]. This waste-valorization process could reduce the environmental and economic costs associated with the precursors while eliminating the need of disposal or incineration of unwanted agricultural by-products[24]. In particular, olive stones are seen as suitable precursors, giving activated carbons with high adsorption capacities, important mechanical strength and low ash content[25].

On the present work, the CH_4 and CO_2 adsorption capacity of three different activated carbons prepared from olive stones under activation conditions are evaluated by means of adsorption isotherms on the pressure range of 0 to 3,3 MPa at two working temperatures (303.15 and 323.15 K). Results are discussed in terms of samples textural properties and surface chemistry.

2. Materials

2.1. Sample Preparation

Three activated carbons were prepared using olive pomace as precursor, two were obtained by physical activation and one by chemical activation. Prior to the activation procedures, the raw materials, provided by an olive oil factory located in Zarzis (Tunisia) were throughly washed with hot distilled water, ambient dried (24 h) and crushed obtaining 1-3 mm particles. The activated carbons preparation method is summarized in this section, while the complete description can be found elsewhere [26].

2.1.1. Physical Activation

Physical activation was carried out by a 2 hours carbonization step at 600 °C under nitrogen flow, followed by the activation step at 750°C. On this step nitrogen was change to either water vapor or carbon dioxide and kept on a constant flux for 6 hours. Samples obtained on this way are denoted as AC-H_2O and AC-CO_2 respectively.

2.1.2. Chemical Activation

The olive stones were immersed in an orthophosporic acid aqueous solution (50% w/w) at the weigh ratio of 1:3. The mixture was kept stiring at 110 °C for a total duration of 9 hours, after this period the solution was filtrated and dried and carbonized at 170 °C for 30 minutes plus 150 min at 410°C. Finally the sample was washed with distilled water and dried at 110 °C. The sample, referred as AC-H_3PO_4 had a chemical activation yield of 33 wt%.

2.2. Samples Properties

The characterization of the obtained activated carbons was done by means of textural properties (such as surface area and pore volume) and surface chemistry, this results can also be found on a

previous work [26]. The obtained textural properties of the three activated carbons are summarized in Table 1.The obtained activated carbons are mainly microporous, with the AC-H$_2$O having also an important mesoporous volume (V$_{meso}$=0.30 cm^3 g^{-1}). The presence of mesoporous volume on water vapor activated carbons due to a higher gasification of the carbon source of the precursor has been previously reported [26,27]. On the other hand, the chemical activated carbon AC-H$_3$PO$_4$ has significantly higher BET surface area (S_{BET}) and micropore volume V_μ that the physical activated ones in agreement with the literature [28].

Table 1. Textural Properties of Carbon Materials

Sample	S_{BET} (m^2 g^{-1})	V_μ N$_2$ (cm^3 g^{-1})	V_{TOT} (cm^3 g^{-1})	V_{meso} N$_2$ (cm^3 g^{-1})
AC-H$_3$PO$_4$	1178	0.45	0.49	0.04
AC-CO$_2$	757	0.30	0.32	0.02
AC-H$_2$O	754	0.28	0.58	0.30

The surface chemistry of the adsorbent can be of great importance for the adsorption process, for this reason the type and quantity of surface oxygenated groups was determined by means of temperature programmed desorption coupled with a mass spectometer (TPD-MS) (see Table 2). The TPD-MS diagrams can be found elsewhere [26]. When increasing the temperature the oxygen surface groups decomposed in the form of carbon monoxide (CO) and carbon dioxide (CO$_2$), with the desoprtion temperature been an indicator on the type of decomposed functional groups, in example the emission of carbon dioxide shows the presence of lactones, carboxilic acids and anhydrides while groups like phenol, ethers and quinones result in carbon monoxide TPD peaks.

Table 2. Cumulated Amounts of the Emmited CO and CO$_2$ During the TPD-MS Analysis of Carbon Materials

Sample	CO (mmol g^{-1})	CO$_2$ (mmol g^{-1})
AC-H$_3$PO$_4$	3.43	0.72
AC-CO$_2$	1.06	0.38
AC-H$_2$O	1.25	0.39

The chemically activated carbon presented the higher amounts of oxygenated groups, mainly carboxilic acids quinones and anhydrides. Among the physically activated carbons, the water vapor activation resulted in more surface oxygen in the form of phenol and carboxilic acids. Meanwhile, carbon dioxide activation resulted in the formation of quinones, lactones and carboxilic acids on the activated carbon surface [26] .

3. Experimental Methodology

3.1. High Pressure Manometric Adsorption Setup

The instrument used in the present study is a High Pressure (HP) manometric device. A schematic view of this "homemade" apparatus is provided in Figure 1. The experimental setup and the measurement principle have been previously described[29,30].

The fundamental elements of this apparatus are the dosing cell, V_{dos}, the adsorption cell, V_{ads} and a MKS pressure transducer baratron type 121 A (0.01% uncertainty in the full scale from vacuum to 3,3 MPa) connected to the dosing cell. The two cells are isolated by spherical valves, thus, limiting the "dead space" volume. The whole system is placed under isothermal conditions through the use of a heating wire controlled by a Eurotherm 3208 PID. Thermocouples located in several points of the instrument allow to check the non-appearance of temperature gradients within the system. This set-up is designed to operate over wide ranges of pressure (0 to 3.3 MPa) and temperatures up to 373,15 K.
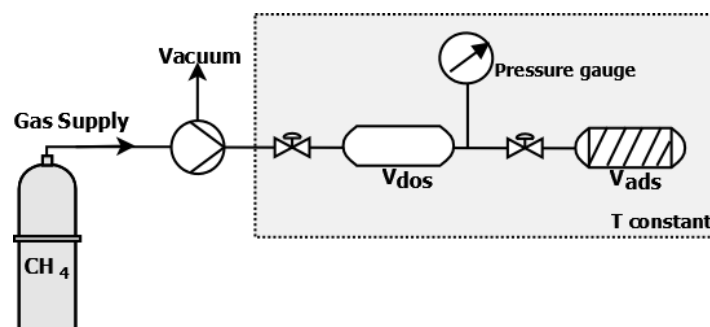
Figure 1. Schematic diagram of the HP/HT manometric adsorption set-up

3.2. Determination of Excess Adsorption

The experimental methodology applied for the adsorption isotherms measurement is based on a mass balance principle. For each working temperature, the accesible volume,or void volume, when an outgassed quantity of the adsorbent was present in the adsorption cell, was estimated by expansion of Helium (He) from the dosing to the adsorption cell. Helium being considered as a non-sorbing gas. The volume of the dosing cell was measured prior to the adsorption isotherms measurement by recording the pressure changes when inserting known quantities of carbon dioxide (CO_2) into the cell at constant temperature, using the NIST Isothermal properties of carbon dioxide the corresponding volume was calculated [31]. The uncertainty on the calculations of the void and adsorption cell volume was always inferior to 0.5%. An outgassing process where the sample was kept under vacuum conditions at 473 K for 10 hours was performed before any experiment. For obtaining the adsorption isotherm an accumulative process was followed, successive doses of the adsorbate (CH_4 or CO_2) were introduced in the dosing cell and expanded into the adsorption cell. An increase of about 3 bars (0.3 MPa) is implemented between each measurement. The stability of the pressure was the chosen indicator of equilibrium conditions.

3.3. Parametrization of Excess Adsorption Isotherms

The excess adsorption isotherms were fitted to a modified Langmuir model:

$$n_{exc} = n_L \frac{p}{p + p_L} \left(1 - \frac{\rho_g(p,T)}{\rho_{ads}} \right) \tag{1}$$

expression in which, n_{exc} is the adsorbed amount of gas (mol kg^{-1}) at p (MPa); p_L is the Langmuir pressure, or pressure at which half of the adsorption sites are occupied (monolayer), n_L is the maximum Langmuir capacity which corresponds to the adsorption amount when all the monolayer is filled, ρ_g is the gas density (kg m^{-3}) at p and T, and ρ_{ads} (kg m^{-3}) the adsorbed phase density, was fixed to be the inverse of the van der Waals volume of each gas or 373 kg m^{-3} for methane and 1027 kg m^{-3} for carbon dioxide [32]. The Langmuir model has the advantage of taking into account the volume of the adsorbed phase it also has a theoretical basis with other models such as Toth and Sips being empirical. Initially developed for low pressures conditions, the Langmuir model can provide a reasonable approximation of the excess adsorption isotherms at higher pressures [17].

The curves fit were obtained by a minimizing process of the root mean square error (RMSE) provided by equation 2 [7]:

$$RMSE = \frac{1}{k} \cdot \sqrt{\sum_{1}^{k}(n_{exp} - n_{calc})^2} \tag{2}$$

Where n_{exp} and n_{calc} are the experimental and calculated adsorption amounts in mol kg^{-1} at a pressure p and k is the number of data points on the adsorption isotherm.

4. Results

The adsorption isotherms of both CH_4 and CO_2 were obtained for the three olive-stones based activated carbons (Figs. 2 and 3) up to a pressure of 3.2 MPa and two working temperatures: 303.15 and 323.15 K with a reproducibility superior to 99% (average absolute deviation of less than 1%). The adsorption isotherms were fitted by the Langmuir two parameters model (see Eq. 1), the obtained fitting parameters and root mean square error (RMSE) are presented in Table 3 (CH_4 adsorption) and Table 4 (CO_2 adsorption). The obtained RMSE values are smaller than 0.09 indicating a good fitting procedure.
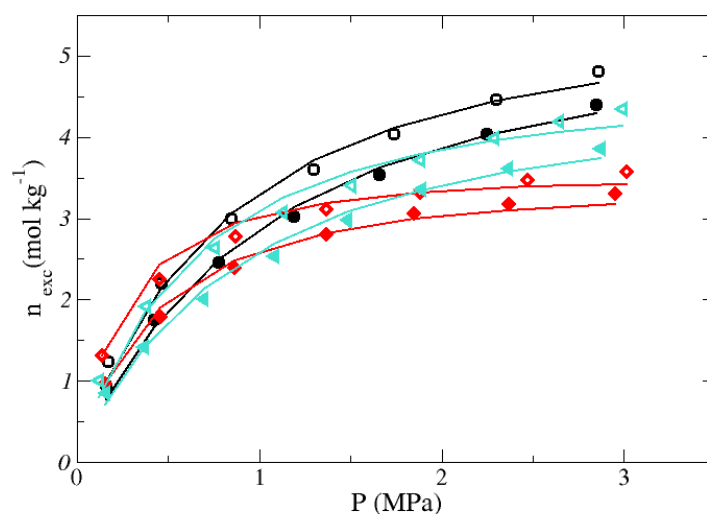

Figure 2. CH_4 Adsorption isotherms at 303.15 K (open symbols) and 323.15 K (filled symbols) of the activated carbons: AC-H_3PO_4 (black circles), AC-CO_2 (red diamonds) and AC-H_2O (turquoise triangles). The obtained Langmuir fitting isotherms are shown by solid lines for each of the adsorption isotherm.

Figure 3. CO_2 Adsorption isotherms at 303.15 K (open symbols) and 323.15 K (filled symbols) of the activated carbons: AC-H_3PO_4 (black circles), AC-CO_2 (red diamonds) and AC-H_2O (turquoise triangles). The obtained Langmuir fitting isotherms are shown by solid lines for each of the adsorption isotherm.
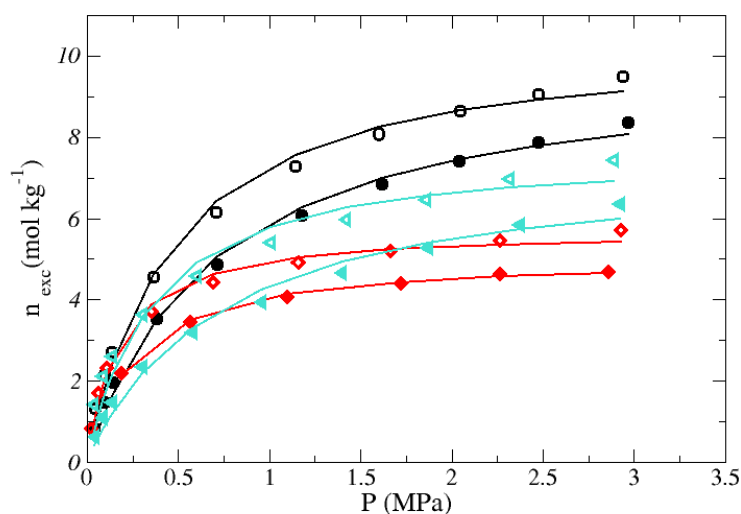
From Tables 3 and 4 and Figures 2 and 3, a higher adsorption of carbon dioxide than methane can be notice for the three AC, this is a normal behavior for activated carbons, the presence of a quadrupole moment on carbon dioxide leads to higher interactions between adsorptive and adsorbent molecules. In addition, the critical temperature (190 K) and critical pressure (4.59 MPa) of methane are much lower than those of carbon dioxide (304.45 K and 7.38 MPa), therefore the carbon dioxide molecules behave as condensable vapor while methane acts as suprecritical gas. For both adsorptives, the chemically activated carbon AC-H_3PO_4 had the higher adsorption capacity, the adsorption tendency vary in the following order: AC-H_3PO_4 (black) > AC-H_2O (turquoise) > AC-CO_2 (red). For all the adsorption isotherms, a higher adsorption temperature resulted in a lower adsorption and lower maximum adsorption capacity which is a classical behavior for physisorption.

Table 3. CH_4 Adsorption Isotherms Langmuir Fitting Parameters

	CH_4 Adsorption			
sample	Temp. (K)	n_L (mol kg^{-1})	ρ_L (MPa)	RMSE
AC-H_3PO_4	303.15	6,518	0,932	0,042
	323.15	6,369	1,182	0,037
AC-CO_2	303.15	3,913	0,273	0,043
	323.15	3,830	0,458	0,031
AC-H_2O	303.15	5,417	0,714	0,067
	323.15	5,301	1,011	0,056

One explanation for the higher adsorption of AC-H_3PO_4 can be given in terms of textural properties of the samples (see Table 1), this chemically activated carbon has both the higher BET surface area and micropore volume, both adsorption enhancing factors. A higher BET surface area means more physisorption available sites, while a linear relationship between the micropore volume of both methane and carbon dioxide has been reported [20,33]. The difference in the methane adsorption

capacity between the physically activated carbons could be attributed to the presence of mesoporosity on the structure of the water vapor activated carbon $AC-H_2O$. Both physically activated carbons have similar BET surface areas and micropore volume, with the only difference being the mesopore volume. In fact, it has been shown that activated carbons that combine both micropores and mesopores can adsorb a significantly higher amount of CH_4 than their totally microporous counterparts [34].

Table 4. CO_2 Adsorption Isotherms Langmuir Fitting Parameters

		CO_2 Adsorption		
sample	Temp. (K)	n_L (mol kg^{-1})	ρ_L (MPa)	*RMSE*
AC-H$_3$PO$_4$	303.15	10,873	0,488	0,080
	323.15	10,254	0,733	0,065
AC-CO$_2$	303.15	5,878	0,181	0,059
	323.15	5,191	0,273	0,020
AC-H$_2$O	303.15	7,968	0,371	0,073
	323.15	7,721	0,772	0,087

If the methane adsorption process by activated carbons is reported to be only influenced by the structural properties of the material, the CO_2 adsorption can also be related to the surface chemistry of the material. The influence of the surface chemistry can be depicted by normalizing the CO_2 adsorption isotherms by the BET surface area (Fig. 4). One could expect that by doing this the adsorption of the chemical activated carbon would still be the most important due to a higher micropore volume. In reality, the $AC-H_2O$ shows the higher adsorption. Chemical activation with phosphoric acid (H_3PO_4) is reported to produce acid activated carbon surfaces[35], which seems to reduce the interactions between the basic surface groups and the carbon dioxide molecules explaning its lower adsorption when the textural effect is eliminated by normalizing the adsorption isotherms by the BET surface area. However, the negative influence of acid surface groups on the $AC-H_3PO_4$ is small compared to the effect of its higher surface area, thus showing a higher adsorption capacity (Table 4).

Among the two physical activated carbons $AC-H_2O$ has the highest quantity of oxygenated surface groups (Table 2), which explains its dominant adsorption when BET normalized. An increase on the CO_2 adsorption capacity upon the presence of oxygen-containing surface functionalities by means of acid-base interactions and hydrogen bonds formation between the adsorbate and the activated carbons surface [36,37]. The high electronegativities of oxygen surface groups due to electron gain from the carbon surface atoms gives them the possibility of electron-donation with the CO_2 adsorbate molecules acting then as basic groups. Furthermore,
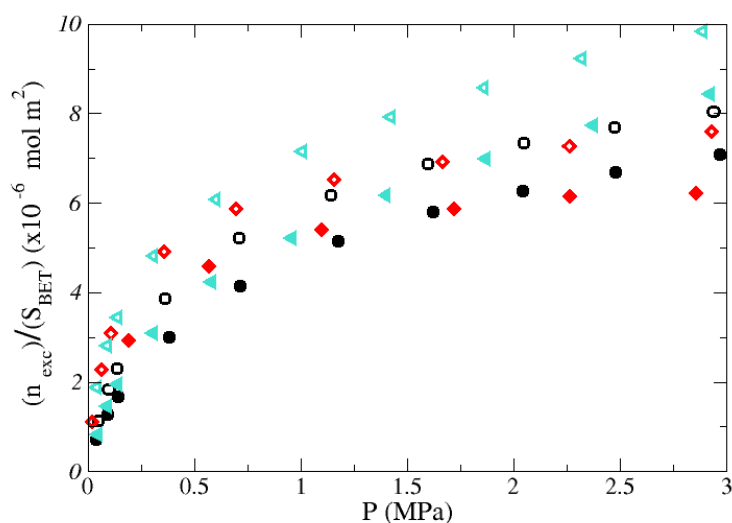
Figure 4. S_{BET} normalized CO_2 Adsorption isotherms at 303.15 K (open symbols) and 323.15 K (filled symbols) of the activated carbons: AC-H_3PO_4 (black circles), AC-CO_2 (red diamonds) and AC-H_2O (turquoise triangles).

5. Conclusions

The effect of the activation method on the adsorption behavior of carbon dioxide and methane was studied. For both adsorptives the higher surface area and micropore volume of the chemically activated carbon resulted in a higher adsorption capacity. The two physically activated carbons had similar surface areas and micropore volume but nevertheless, the water vapor activated carbon presented higher adsorption. Methane adsorption seems to be enhanced by the presence of mesopores on the water vapor activated carbon which facilitates the gas difussion into the micropores. For carbon dioxide adsorption the acid-basic interactions between the adsorptive molecules and the oxygen surface groups are thought to enhance the adsorption capacity.

Author Contributions: Samples preparation and characterization:Imen Ghouma, Camelia Matei Ghimbeu and Mejdi Jeguirim. Adsorption isotherms: Deneb Peredo-Mancilla, Cecile Hort and David Bessieres. Writting of the article: Deneb Peredo-Mancilla. Revision of the article content: All of the authors.

Conflicts of Interest: The authors declare no conflict of interest.

References

1. European Comission. Paris Agreement.
2. European Comission. Renewable Energy. Moving towards a low carbon economy.
3. Starr, K.; Villalba, G.; Gabarrell, X. Upgraded biogas from municipal solid waste for natural gas substitution and CO_2 reduction - A case study of Austria, Italy, and Spain. *Waste Management* **2015**, *38*, 105–116. doi:10.1016/j.wasman.2015.01.001.
4. Sahota, S.; Shah, G.; Ghosh, P.; Kapoor, R.; Sengupta, S.; Singh, P.; Vijay, V.; Sahay, A.; Vijay, V.K.; Thakur, I.S. Review of trends in biogas upgradation technologies and future perspectives. *Bioresource Technology Reports* **2018**, *1*, 79–88. doi:10.1016/j.biteb.2018.01.002.
5. EBA European Biogas Association. EBA statictical report 2017 published soon.
6. Angelidaki, I.; Treu, L.; Tsapekos, P.; Luo, G.; Campanaro, S.; Wenzel, H.; Kougias, P.G. Biogas upgrading and utilization: Current status and perspectives. *Biotechnology Advances* **2018**, *36*, 452–466. doi:10.1016/j.biotechadv.2018.01.011.

7. Jiang, Y.; Ling, J.; Xiao, P.; He, Y.; Zhao, Q.; Chu, Z.; Liu, Y.; Li, Z.; Webley, P.A. Simultaneous biogas purification and CO_2 capture by vacuum swing adsorption using zeolite NaUSY. *Chemical Engineering Journal* **2018**, *334*, 2593–2602. doi:10.1016/j.cej.2017.11.090.

8. Gong, H.; Lee, S.S.; Bae, T.H. Mixed-matrix membranes containing inorganically surface-modified 5A zeolite for enhanced CO_2/CH_4 separation. *Microporous and Mesoporous Materials* **2017**, *237*, 82–89. doi:10.1016/j.micromeso.2016.09.017.

9. Kennedy, D.A.; Tezel, F.H. Cation exchange modification of clinoptilolite – Screening analysis for potential equilibrium and kinetic adsorption separations involving methane, nitrogen, and carbon dioxide. *Microporous and Mesoporous Materials* **2018**, *262*, 235–250. doi:10.1016/j.micromeso.2017.11.054.

10. Son, S.J.; Choi, J.S.; Choo, K.Y.; Song, S.D.; Vijayalakshmi, S.; Kim, T.H. Development of carbon dioxide adsorbents using carbon materials prepared from coconut shell. *Korean Journal of Chemical Engineering* **2005**, *22*, 291–297. doi:10.1007/BF02701500.

11. Rocha, L.A.; Andreassen, K.A.; Grande, C.A. Separation of CO_2/CH_4 using carbon molecular sieve (CMS) at low and high pressure. *Chemical Engineering Science* **2017**, *164*, 148–157. doi:10.1016/j.ces.2017.01.071.

12. Arya, A.; Divekar, S.; Rawat, R.; Gupta, P.; Garg, M.O.; Dasgupta, S.; Nanoti, A.; Singh, R.; Xiao, P.; Webley, P.A. Upgrading biogas at low pressure by vacuum swing adsorption. *Industrial and Engineering Chemistry Research* **2015**, *54*, 404–413. doi:10.1021/ie503243f.

13. Samarasinghe, S.A.; Chuah, C.Y.; Yang, Y.; Bae, T.H. Tailoring CO_2/CH_4 separation properties of mixed-matrix membranes via combined use of two- and three-dimensional metal-organic frameworks. *Journal of Membrane Science* **2018**, *557*, 30–37. doi:10.1016/j.memsci.2018.04.025.

14. Zacharia, R.; Gomez, L.F.; Chahine, R.; Cossement, D.; Benard, P. Thermodynamics and kinetics of CH_4/CO_2 binary mixture separation by metal-organic frameworks from isotope exchange and adsorption break-through. *Microporous and Mesoporous Materials* **2018**, *263*, 165–172. doi:10.1016/j.micromeso.2017.12.011.

15. Cheng, Y.; Wang, X.; Jia, C.; Wang, Y.; Zhai, L.; Wang, Q.; Zhao, D. Ultrathin mixed matrix membranes containing two-dimensional metal-organic framework nanosheets for efficient CO_2/CH_4 separation. *Journal of Membrane Science* **2017**, *539*, 213–223. doi:10.1016/j.memsci.2017.06.011.

16. Yao, K.X.; Chen, Y.; Lu, Y.; Zhao, Y.; Ding, Y. Ultramicroporous carbon with extremely narrow pore distribution and very high nitrogen doping for efficient methane mixture gases upgrading. *Carbon* **2017**, *122*, 258–265. doi:10.1016/j.carbon.2017.06.073.

17. Koonaphapdeelert, S.; Moran, J.; Aggarangsi, P.; Bunkham, A. Low pressure biomethane gas adsorption by activated carbon. *Energy for Sustainable Development* **2018**, *43*, 196–202. doi:10.1016/j.esd.2018.01.010.

18. Saha, D.; Nelson, K.; Chen, J.; Lu, Y.; Ozcan, S. Adsorption of CO_2 ,CH_4 , and N_2 in Micro-Mesoporous Nanographene: A Comparative Study. *Journal of Chemical & Engineering Data* **2015**, *60*, 2636–2645. doi:10.1021/acs.jced.5b00291.

19. Vilella, P.C.; Lira, J.A.; Azevedo, D.C.; Bastos-Neto, M.; Stefanutti, R. Preparation of biomass-based activated carbons and their evaluation for biogas upgrading purposes. *Industrial Crops and Products* **2017**, *109*, 134–140. doi:10.1016/j.indcrop.2017.08.017.

20. Serafin, J.; Narkiewicz, U.; Morawski, A.W.; Wróbel, R.J.; Michalkiewicz, B. Highly microporous activated carbons from biomass for CO_2 capture and effective micropores at different conditions. *Journal of CO2 Utilization* **2017**, *18*, 73–79. doi:10.1016/j.jcou.2017.01.006.

21. Yadavalli, G.; Lei, H.; Wei, Y.; Zhu, L.; Zhang, X.; Liu, Y.; Yan, D. Carbon dioxide capture using ammonium sulfate surface modified activated biomass carbon. *Biomass and Bioenergy* **2017**, *98*, 53–60. doi:10.1016/j.biombioe.2017.01.015.

22. Hao, W.; Björkman, E.; Lilliestråle, M.; Hedin, N. Activated carbons prepared from hydrothermally carbonized waste biomass used as adsorbents for CO_2. *Applied Energy* **2013**, *112*, 526–532. doi:10.1016/j.apenergy.2013.02.028.

23. González-García, P. Activated carbon from lignocellulosics precursors: A review of the synthesis methods, characterization techniques and applications. *Renewable and Sustainable Energy Reviews* **2018**, *82*, 1393–1414. doi:10.1016/j.rser.2017.04.117.

24. Gil, R.R.; Ruiz, B.; Lozano, M.S.; Fuente, E. Influence of the pyrolysis step and the tanning process on KOH-activated carbons from biocollagenic wastes. Prospects as adsorbent for CO_2 capture. *Journal of Analytical and Applied Pyrolysis* **2014**, *110*, 194–204. doi:10.1016/j.jaap.2014.09.001.

25.   Álvarez-Gutiérrez, N.; García, S.; Gil, M.V.; Rubiera, F.; Pevida, C. Towards bio-upgrading of biogas: Biomass waste-based adsorbents. *Energy Procedia* **2014**, *63*, 6527–6533. doi:10.1016/j.egypro.2014.11.688.

26.   Ghouma, I.; Jeguirim, M.; Sager, U.; Limousy, L.; Bennici, S.; Däuber, E.; Asbach, C.; Ligotski, R.; Schmidt, F.; Ouederni, A. The potential of activated carbon made of agro-industrial residues in NOx immissions abatement. *Energies* **2017**, *10*. doi:10.3390/en10101508.

27.   Román, S.; Ledesma, B.; Álvarez-Murillo, A.; Al-Kassir, A.; Yusaf, T. Dependence of the microporosity of activated carbons on the lignocellulosic composition of the precursors. *Energies* **2017**, *10*. doi:10.3390/en10040542.

28.   Song, T.; Liao, J.M.; Xiao, J.; Shen, L.H. Effect of micropore and mesopore structure on CO_2 adsorption by activated carbons from biomass. *Xinxing Tan Cailiao/New Carbon Materials* **2015**, *30*, 156–166. doi:10.1016/S1872-5805(15)60181-0.

29.   Ortiz Cancino, O.P.; Peredo Mancilla, D.; Pozo, M.; Pérez, E.; Bessieres, D. Effect of Organic Matter and Thermal Maturity on Methane Adsorption Capacity on Shales from the Middle Magdalena Valley Basin in Colombia. *Energy and Fuels* **2017**, *31*, 11698–11709. doi:10.1021/acs.energyfuels.7b01849.

30.   Peredo-Mancilla, D.; Hort, C.; Jeguirim, M.; Ghimbeu, C.M.; Limousy, L.; Bessieres, D. Experimental Determination of the CH_4 and CO_2 Pure Gas Adsorption Isotherms on Different Activated Carbons. *Journal of Chemical & Engineering Data* **2018**, p. acs.jced.8b00297. doi:10.1021/acs.jced.8b00297.

31.   U.S. Secretary of Commerce. Isothermal Properties for Carbon Dioxide, 2017.

32.   Gensterblum, Y.; Merkel, A.; Busch, A.; Krooss, B.M. High-pressure CH_4 and CO_2 sorption isotherms as a function of coal maturity and the influence of moisture. *International Journal of Coal Geology* **2013**, *118*, 45–57. doi:10.1016/j.coal.2013.07.024.

33.   Lozano-Castelló, D.; Cazorla-Amorós, D.; Linares-Solano, A.; Quinn, D.F. Influence of pore size distribution on methane storage at relatively low pressure: Preparation of activated carbon with optimum pore size. *Carbon* **2002**, *40*, 989–1002. doi:10.1016/S0008-6223(01)00235-4.

34.   Casco, M.E.; Martínez-Escandell, M.; Gadea-Ramos, E.; Kaneko, K.; Silvestre-Albero, J.; Rodríguez-Reinoso, F. High-pressure methane storage in porous materials: Are carbon materials in the pole position? *Chemistry of Materials* **2015**, *27*, 959–964. doi:10.1021/cm5042524.

35.   Nowicki, P.; Wachowska, H.; Pietrzak, R. Active carbons prepared by chemical activation of plum stones and their application in removal of NO_2. *Journal of Hazardous Materials* **2010**, *181*, 1088–1094. doi:10.1016/j.jhazmat.2010.05.126.

36.   Liu, Y.; Wilcox, J. Molecular Simulation Studies of CO_2 Adsorption by Carbon Model Compounds for Carbon Capture and Sequestration Applications. *Environmental Science & Technology* **2013**, *47*, 95–101. doi:10.1021/es3012029.

37.   Xing, W.; Liu, C.; Zhou, Z.; Zhou, J.; Wang, G.; Zhuo, S.; Xue, Q.; Song, L.; Yan, Z. Oxygen-containing functional group-facilitated CO_2 capture by carbide-derived carbons. *Nanoscale Research Letters* **2014**, *9*, 1–8. doi:10.1186/1556-276X-9-189.